Hindawi Publishing Corporation
Journal of Nanomaterials
Volume 2014, Article ID 298619, 9 pages
http://dx.doi.org/10.1155/2014/298619

Research Article

Photocatalytic Activity Enhancement of Anatase TiO_2 by Using TiO

Zhenrui Chen, Wei Zhong, Zhutian Liang, Weiqian Li, Guannan He, Yinzhen Wang, Wei Li, Yuandong Xie, and Qinyu He

Laboratory of Quantum Engineering and Quantum Materials, Advanced Material Laboratory, School of Physics Department and Telecommunication Engineering, South China Normal University, Guangzhou 510006, China

Correspondence should be addressed to Qinyu He; gracylady@163.com

Received 28 December 2013; Accepted 21 January 2014; Published 16 March 2014

Academic Editor: Chuanfei Guo

We employed high-energy ball-milling technique to fabricate TiO/TiO_2 heterogeneous nanostructures. XRD proved the existence of TiO/TiO_2 heterogeneous structures. SEM and HRTEM investigation evidenced that the mean particle size and mean grain size of the as-prepared samples are 23 nm and 13 nm, respectively. UV-Vis spectra exhibited that TiO has enhanced the visible light absorption of TiO_2 and has changed the E_g of TiO_2. UPS examination indicated that the electron work function (EWF) of TiO is higher than that of TiO_2. Photocatalytic degradation experiments revealed that an appropriate TiO content can enhance the photocatalytic activity of pure anatase TiO_2. The best photocatalytic activity of TiO/TiO_2 heterogeneous nanostructures is even better than that of Au-deposited TiO_2 by keeping high degradation efficiency of 93%. The internal electrical field producing in TiO/TiO_2 heterogeneous nanostructures was considered to be dominantly responsible for the enhanced photocatalytic activity. Therefore, the substitution of TiO with noble metal in TiO_2 will be widely used in the future due to its low cost. This study also provides a clear direction of enhancing photocatalytic activity of TiO_2: incorporating a guest compound into TiO_2 with an appropriate content if the compound has much higher electron work function than that of TiO_2.

1. Introduction

Anatase titanium dioxide (TiO_2) has been proved to be the most effective and suitable photocatalyst for the degradation of environment pollutants due to its low cost, nontoxicity, availability, relatively high efficiency, structural stability, and so forth [1]. However, its low photocatalytic activity limits the application. Therefore, it is a critical issue to enhance its photocatalytic activity to realize its photocatalytic application. From many works, it can be found that the photocatalytic activity of the photocatalysts is strongly dependent on their structures [2–4]. And it was also reported that nanosized heterogeneous structures can enhance the quantum yield and therefore can enhance the photocatalytic activity of anatase TiO_2 [5, 6]. The reason is that the heterogeneous structures in the interface produce internal fields and the recombination of photogenerated carriers can be suppressed [5, 6]. The most effective approach to suppress charge-carrier recombination in the photocatalysis process is to incorporate noble metal (Au, Ag, or Pt) into TiO_2 [7–10]. In these systems, the electron work functions (EWF) of the noble metals are much higher than that of TiO_2. Therefore, larger internal fields can be produced in these systems. In addition, the photogenerated carriers tend to be transported from TiO_2 to the noble metals and easily transfer to the sites needed for the deoxidized reactions [11]. As a result, the photocatalytic activity of TiO_2 can be improved by deposited noble metals. From the above analysis, one can find a route to increase the photocatalytic activity of TiO_2: incorporating a second compound which has higher EWF than TiO_2 and has high electrical conductivity.

In this work, we added TiO, rather than the noble metals, into commercial anatase TiO_2 to improve the photocatalytic activity of TiO_2 to lower the cost of photocatalyst. TiO has low cost, safety, and metallic properties [12, 13]. It is expected to have higher EWF than TiO_2 like most metals. If anatase TiO_2 is incorporated with TiO, it would have high photocatalytic activity of photocatalysis due to TiO/TiO_2 heterogeneous structures. In order to mix TiO with TiO_2 particle evenly,

a high-energy ball-milling process was adopted [14]. As presumed above, an enhanced photocatalytic activity has been found in the as-prepared TiO-TiO_2 system.

2. Experimental Procedures

2.1. Preparation of Photocatalyst. The planetary ball-milling apparatus used is commercially available (KEQ-0.4 L, Qidonghongchun Company, China). A zirconia (ZrO_2) milling vessel and ZrO_2 milling balls were used to grind the needed particles. The rotating speed was 800 rpm. The purchased TiO (CP, 99.9%, 1-2 μm, Alden Company, China) and TiO_2 (CP, 99.9%, 1-2 μm, Alden Company) were independently ball-milled for 60 hrs. Then the as-ball-milled TiO powders and TiO_2 powders were mixed according to the TiO-to-TiO_2 molar ratio: 1/1000, 10/1000, 20/1000, 50/1000, and 100/1000 (denoted as TT1, TT10, TT20, TT50, and TT100, resp.). The mixtures were followed by 60 hr ball milling in the above-mentioned ball-milling machine. In order to isolate the effects of ball milling from that of TiO on photocatalytic activity of the TiO_2, a pure TiO (denoted as "PTiO") and pure TiO_2 (denoted as "TiO_2") ball-milled for 120 hrs were prepared as comparisons.

2.2. Photocatalyst Characterization. The X-ray diffraction (XRD, X'Pert Pro, Panalytical) was employed to investigate the phases of as-ball-milled powders with slow scanning speed ($2^\circ\,\mathrm{min}^{-1}$). The scanning electron microscopy (SEM, Zeiss Ultra 55, Carl Zeiss) was used to examine the micrographs of the particles of as-prepared powders. The high resolution electron microscopy (HRTEM, JEM-2100HR, JEOL) was utilized to observe the grain size. UV-Vis diffuse reflection spectra (DRS) were obtained using a spectrophotometer Shimadzu 2550PC and the reflection data were converted to absorbance through the standard Kubelka-Munk method. The X-ray photoelectron spectroscopy/ESCA (Esclab 250, Thermo Fisher Scientific) was obtained by using UPS mode and He (I) irradiation to examine the EWF and valence band maximum (VBM) of as-ball-milled powders. We also measured the electrical properties (ZEM-3, Ulvac-Riko) of as-ball-milled powders by testing the pressed powders (at room temperature, 200 MPa).

2.3. Photocatalytic Experiments. The photocatalytic activity of the samples was evaluated by measuring the degradation rates of methylene orange (MO) solution (10 mg L^{-1}) under ultraviolet-visible (UV-Vis) light irradiation [15]. The MO concentration was monitored by a UV-Vis spectrometer. The photocatalytic reaction was performed in a quartz reactor (XQ350W, Shanghai Lansheng Company). A 350 W xenon-arc lamp, with similar emitting spectrum to the sun, was used as light resource, which was located at a distance of 10 cm from the quartz reactor. A stirring bar, MO aqueous solution, and TiO_2 dispersion solution were placed in a quartz cuvette. Before photogradation, the solution was stirred in dark for 40 mins to achieve adsorTiOn/desorTiOn equilibrium. The irradiation time ranged from 0 to 120 min. At given time intervals (15 mins), about 3.5 mL of MO solution was taken out and centrifuged for 15 min. After removing the nanoparticles by filtration, the MO solution was measured by the UV-Vis spectrophotometer. The concentration of the MO solution was analyzed by checking the absoption peak around 464 nm, which is attributed to the Azo functional group (–N=N–) of MO [15]. According to the Beer-Lambert law, the absorbance of MO solution is proportional to its concentration. The change of MO concentration can thus be evaluated by the intensity change of the absoption peak around 464 nm.

The degradation rate (E_d) of MO is expressed in the following equation [16, 17]:

$$\begin{aligned} E_d\,(\%) &= \frac{C_0 - C}{C_0} \times 100\% \\ &= (A_0 - A) - A_0 \times 100\%, \end{aligned} \tag{1}$$

where C_0 is the concentration of MO after absoption equilibrium in the dark, A_0 is the corresponding absorbance intensity of MO after absoption equilibrium in the dark, C is the concentration of MO at reaction time t (min), and A is the corresponding absorbance intensity of MO at reaction time t (min).

3. Results and Discussion

3.1. Phases, Grain Size, and Particle Size. Figure 1 showed the XRD patterns of the as-prepared samples. It shows that there is only anatase phase (JCPDS file number 21-1272) in PTiO_2 while in TiO-incorporated TiO_2 the majority is anatase TiO_2 and the minority is the incorporated TiO (JCPDS file number 08-0117). And the peak positions of anatase TiO_2 have not been changed by the incorporated TiO. The diffraction peaks at (2θ) 25.4°, 37°, 37.9°, 38.7°, 47.9°, 53.9°, 54.9°, 62.6°, 68.8°, 70.3°, 75°, and 76.2° are attributed to (101), (103), (104), (112), (200), (105), (211), (204), (116), (220), (215), and (301) faces of anatase TiO_2, respectively. The diffraction peaks at (2θ) 37.2°, 43.2°, 62.8°, 75.4°, and 79.4° can be ascribed to (111), (200), (220), (311), and (222) faces of TiO. It can be found that the more the TiO contained in TiO-incorporated TiO_2 is, the higher the diffraction peak at 43.2° representing TiO is. Clearly, the incorporated TiO has not changed the peak positions of anatase TiO_2. TiO and TiO_2 just mixed with each other and formed a large number of heterogeneous structures TiO/TiO_2 in host TiO_2 powders after the high-energy ball milling.

The grain size of the as-prepared samples (Table 1) was estimated according to the Debye-Scherrer equation $D = k\lambda/\beta\cos(\theta)$ [18]. From Table 1, it can be seen that there is no effect of the incorporated TiO on the grain size of anatase TiO_2. All the grain sizes of the as-prepared samples are 13~14 nm. The grain size observed under HRTEM (Figure 2) is also about 13 nm. The two data agree very well.

SEM investigation (Figure 3) shows that the mean particle size of the as-prepared samples is 23 nm. And all the particle

Table 1: Mean grain size of the as-prepared samples calculated from XRD by the Debye-Scherrer equation [18].

Sample number	TiO_2	TT1	TT10	TT20	TT50	TT100	PTiO
Grain size (nm)	13.65	13.91	13.43	13.27	13.77	13.69	13.75

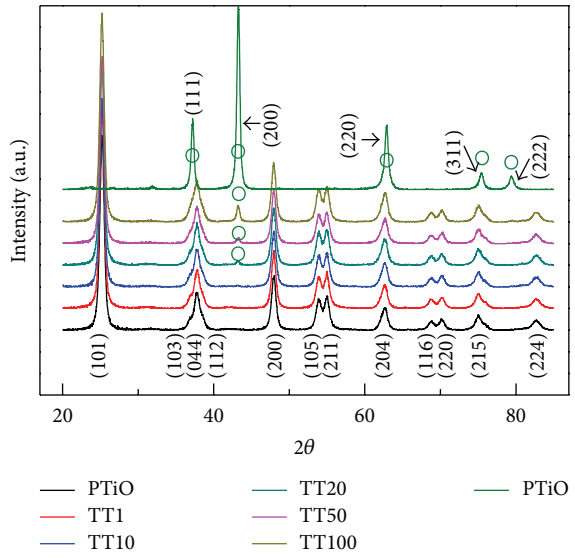

Figure 1: XRD of the as-prepared samples.

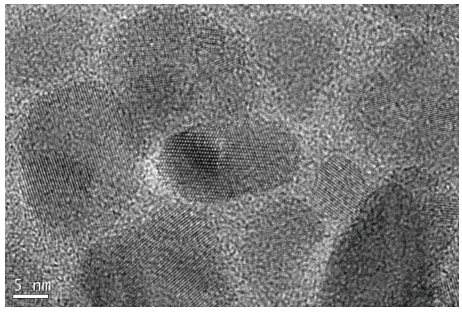

Figure 2: Representative HRTEM image of the as-prepared samples, clearly showing mean grain size around 13 nm.

sizes of the as-prepared samples are very close. Therefore, the incorporated TiO has no effects on the particle size of anatase TiO_2.

3.2. Energy Band Characterization: UV-Vis Absoption, Energy Band Gap (E_g), EWF, and Electrical Conductivity (σ)

3.2.1. UV-Vis Spectrum and E_g. Figure 4 shows the UV-Vis absoption spectra of the as-prepared samples in the range of 220~800 nm obtained by calculating the absoption coefficient A from the obtained DRS according to [19]

$$A = \frac{1}{R(\infty)}, \tag{2}$$

where $R(\infty)$ is the absolute reflection ratio (%). In our work, we substitute $R(\infty)$ with R_e which is the relative reflection ratio by comparing the diffuse reflection ratios (DR) of the as-prepared samples with that of pure $BaSO_4$; that is,

$$A \approx \frac{1}{R_e}. \tag{3}$$

Figure 4 indicates that the A-s of as-prepared samples in visible light (VL) spectrum increase with increasing TiO and increase with increasing wavelength of VL. The increasing absoption with increasing wavelength is characteristic of absorbing properties of free carriers because TiO has metallic properties. But generally, free carriers can strongly absorb infrared light (intraband free-carrier absoption (FCA)) not visible light and are characteristic of increasing absoption with increasing wavelength [20]. Apparently, the intraband FCA has been blue-shifted to the VL range. This implies a great extension of conduction band in the TiO-incorporated TiO_2. The blue shift of intraband FCA could be related to the internal fields which exist in TiO/TiO_2 heterogeneous nanostructures. Detailed discussion will be performed in the next text. The absoption of the as-prepared samples in VL suggests that the incorporated TiO can extend the light absoption region of TiO_2 to VL and improve the UV-Vis absoption efficiency of the samples.

Because there is no strong energy dependence of optical absoption coefficient of the as-prepared near absoption edge in Figure 4, the as-prepared samples should have direct band gap [21, 22]. In other people's works, the nanosized anatase TiO_2 was also found to have direct band gap [23]. Furthermore, anatase TiO_2 is an N-type semiconductor [24, 25]. The optical energy band gap (E_g, eV) can be estimated by using the Kubelka-Munk function ($F(R)$), as expressed by

$$F(R) = \frac{(1-R)^2}{2R}. \tag{4}$$

We substituted R with R_e. The band gap (E_g, eV) was the crossing point between the line extrapolated from the linear part and the x-axis of the plot of $[F(R_\infty)h\nu]^2$ as a function of energy of light ($h\nu$, eV), that is, $[F(R_\infty)h\nu]^{1/2} \sim h\nu$ curve (Figure 5) [23]. Table 2 is the E_g-s of the as-prepared samples (excluding PTiO since it is metallic conduction). It can be seen that all of the E_g-s of the as-prepared samples are larger than 3.4 eV. The maximum E_g is that of TT10, 3.504 eV. The E_g-s of the as-prepared samples would increase with increasing TiO at first and then decrease with increasing TiO. We have not found the exact reason for the E_g-s variation of the as-prepared samples with TiO content. But we guess that the probable reason is that the internal fields from the nanosized TiO/TiO_2 heterogeneous structures have bent the energy band and energy gap [11].

Table 2: The estimated E_g of the as-prepared samples from $[F(R_\infty)h\nu]^2 \sim h\nu$ curve based on DRS results.

Sample number	TiO_2	TT1	TT10	TT20	TT50	TT100
E_g (eV)	3.469	3.485	3.504	3.494	3.479	3.469

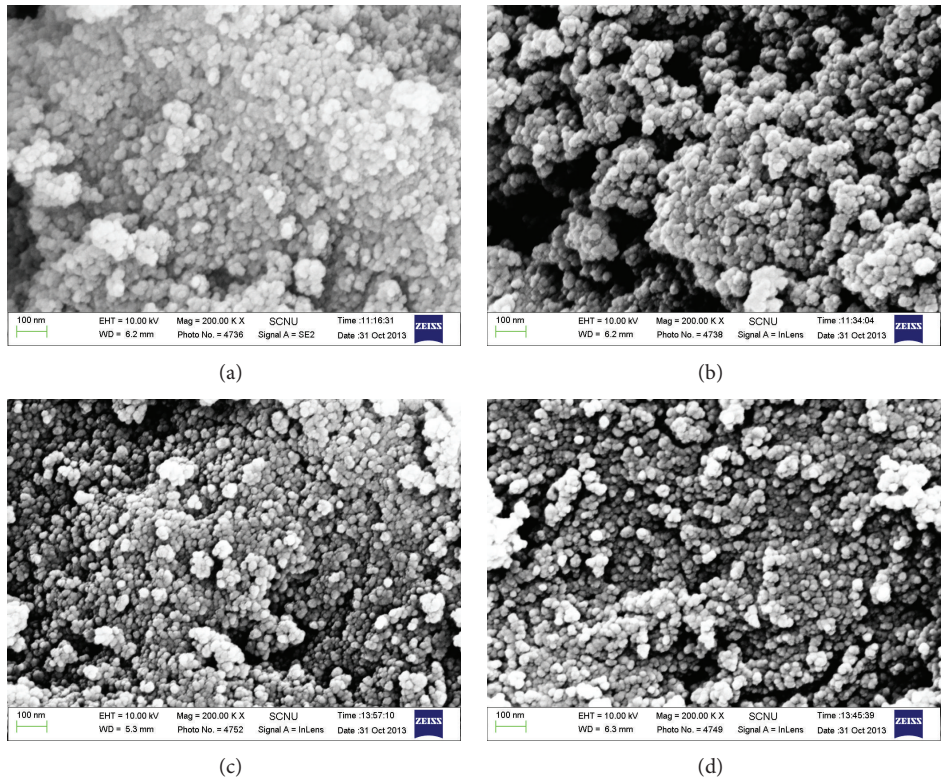

Figure 3: Typical SEM images of (a) TiO_2, (b) TT1, (c) TT20, and (d) PTiO, clearly showing that the partice size of the as-prepared samples is very close and around 23 nm.

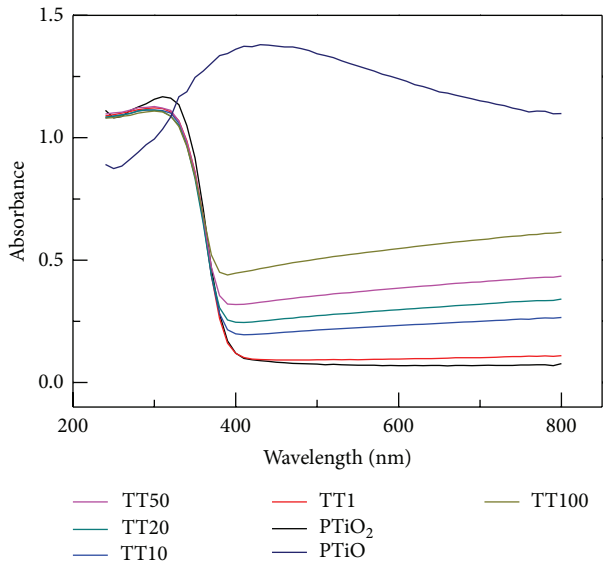

Figure 4: Absoption of the as-prepared samples obtained from the as-measured UV-Vis DRS.

It is known from the previous work that the optical E_g of TiO_2 is related to the measuring method (absoption spectrum/reflection spectrum), doping, processing technique, material form and particle size, and so forth. Therefore, the reported optical E_g-s of TiO_2 range widely, for example, from 2.99 eV to 3.6 eV [26–29]. But the most reported optical E_g is 3.0–3.2 eV [26, 27]. The large E_g in this work mainly results from the small grain size of ~13 nm in the as-prepared samples, which has strong size effects [29, 30]. But the variation of E_g with the content of TiO cannot be ascribed to size effect because the grain size and particle size of all the samples are very close. And the processing procedure and parameters are identical among all the samples. The only different factor is the content of the incorporated TiO. Therefore, the internal fields generated due to heterogeneous structures TiO/TiO_2 should be responsible for it as discussed above.

3.2.2. Electrical Conductivity and EWF. Table 3 gives the σ and the Seebeck coefficients (S) of the as-prepared samples. Because some samples could not be detected by ZEM-3 due to too low electricity, their σ-s and S are denoted by "N."

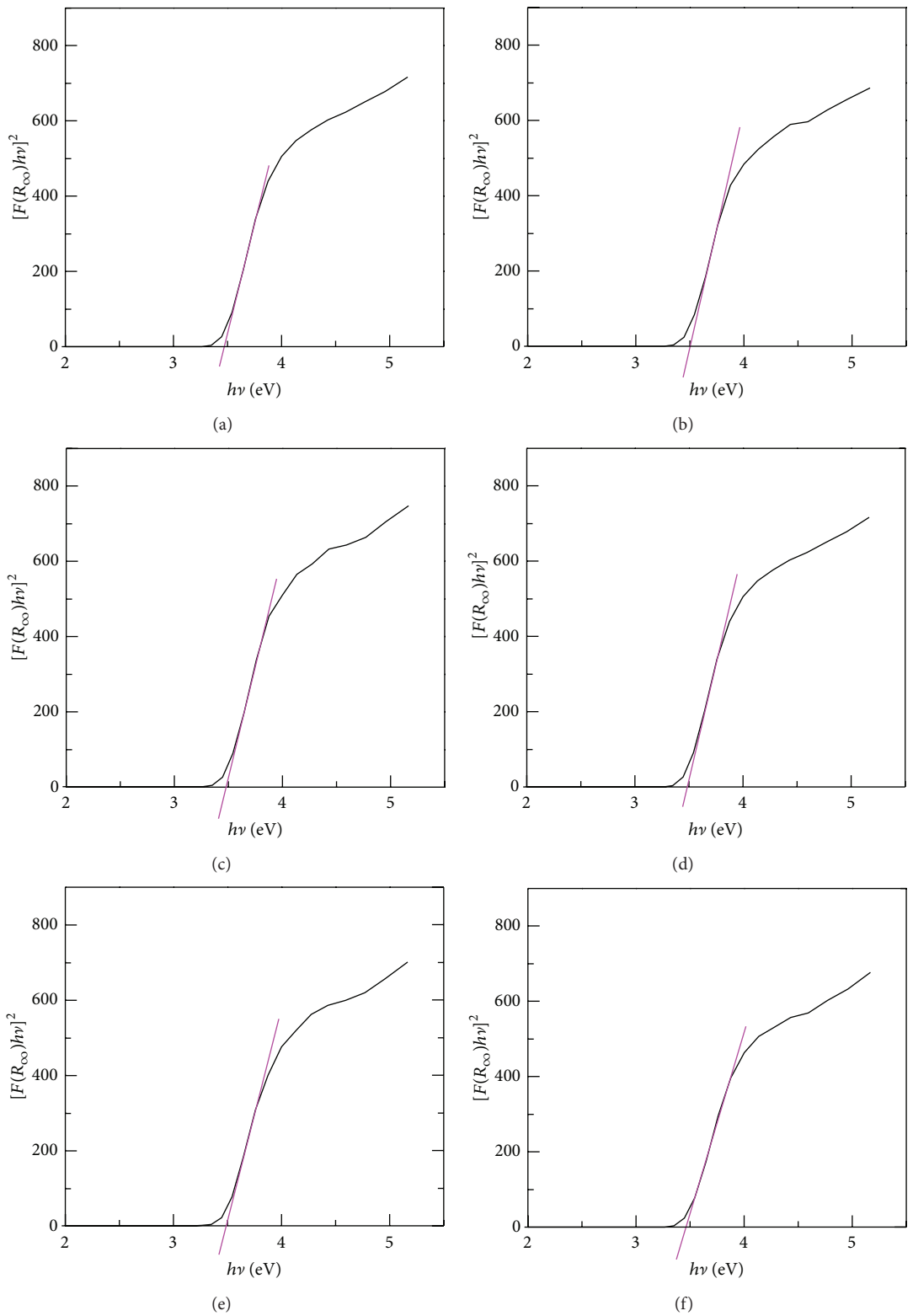

Figure 5: $[F(R_\infty)h\nu]^2 \sim h\nu$ curve of (a) TiO_2, (b) TT1, (c) TT10, (d) TT20, (e) TT50, and (f) TT100.

Table 3: The σ and S of the as-prepared samples measured by ZEM-3. Because some samples could not be detected by ZEM-3 due to too low σ, their σ-s and S are denoted by "N."

Sample number	PTiO	TiO_2	TT1	TT10	TT20	TT50	TT100
σ ($S\,m^{-1}$)	86.5	N	N	N	N	N	N
S ($\mu V\,k^{-1}$)	$-9.42E-06$	N	N	N	N	N	N

From Table 3, it can be seen that only the σ of PTiO can be detected by ZEM-3 due to loose contact between particles in the as-prepared samples since the bulk samples for measuring electrical properties are pressed at room temperature with pressure of 200 MPa. The tested σ of PTiO is 86.5 $S\,m^{-1}$ and the S is close to 0 with negative sign. From the S sign of PTiO, it can be seen that PTiO is a weak N-type semiconductor, suggesting a little bit oxidization in PTiO during high-energy ball milling. On the other hand, previous work presents the fact that pure anatase $PTiO_2$ is a natural N-type semiconductor [24, 25].

Figure 6 is the UPS spectra for PTiO and TT20. The spectra have been referenced to the Fermi level (E_F) of the gold reference sample. During UPS experiment, a bias voltage of −5 V has been added. The EWF, which is the minimum energy required to move electrons at the Fermi energy level from inside a metal or semiconductor to its surface with zero-kinetic energy, equals to the difference between the onset of the measured UPS spectra and 5 eV. While the valence band maximum (E_{VBM}) equals 26.22 eV, the cutoff on the high energy side of UPS spectra. Figure 6(a) combines the UPS spectra of PTiO and those of TT20. Figures 6(b) and 6(c) show the five fitted Gaussian peaks of UPS spectra for PTiO and TT20, respectively. The fitted peaks were based on the expected contributions from the molecular orbitals that comprise the valence bonding states, respectively [31]. Figure 6(a) indicates that valence band of PTiO has been apparently changed after being ball-milled with TiO_2. This is another proof that the energy band of TiO_2 has been changed by the incorporated TiO. The EWF of PTiO is 3.01 eV, while that of TT20 is 1.54 eV. The E_{VBM} of PTiO is 2.67 eV, while that of TT50 is 3.08 eV. Apparently, the EWF of TiO_2 is different from that obtained in other works [31]. It can be attributed to the band bending arising from nanosized TiO/TiO_2 heterogeneous structures [11, 32]. We guess that the EWF of TiO_2 is less than that of PTiO. In the nanosized heterogeneous TiO/TiO_2 structures, the E_F is aligned to the level which is between the EWF of PTiO and that of TiO_2. Therefore, the EWF of TT20 is less than that of TiO and larger than that of TiO_2. The above-mentioned two proofs that there are internal fields are powerful support for the assumTiOn about the EWF of TiO and TiO_2. Actually, the presence of a large number of space charge regions has made the crystal field and the EWF of free electrons, of TT20 different from that of pure TiO and that of pure TiO_2 [32].

3.3. Photoactivity. Figure 7 is the photocatalytic degradation of MO solution (10 mg L^{-1}) by the as-prepared samples under UV-Vis irradiation. It can be seen from Figure 7(a) that, at the beginning irradiation for 70 mins, the degradation efficiencies (DE) reduce as the order of TT20, TT10, TT50, and TT1 (very close), TiO_2, and PTiO. Among the six samples, the PTiO possesses far lower DE than the others. However, the maximum DE of all samples except PTiO reach an identical value ~93% after 75 mins. Therefore, we can conclude that the presence of the incorporated TiO has not enhanced the final DE of nanosized TiO_2 but has improved the photocatalytic activity of the nanosized TiO_2 samples. It can be clearly seen that, before 38.5 mins, the PDRs of MO solution by the as-prepared samples reduce as the same order as that of DE, that is, TT20, TT10, TT50, and TT1 (very close), TT100, TiO_2, and PTiO. But after the irradiation for 38 mins, the order of PDR is turned over as TiO_2, TT100, TT50, and TT1, and TT20 (PTiO is an exceTiOn and always is close to 0). This phenomenon can be understood from the view of point that the PDR is related to the MO concentration: when the MO solution is low, the larger the MO concentration, the larger the PDR [33, 34]. After 38 mins, the residual MO concentration photocatalyzed by the as-prepared samples (excluding PTiO) reduces as the order of TiO_2, TT100, TT50, and TT1, and TT20, the same order as that of PDR.

We here explain why TT20 has a maximum DE and PDR before 38 mins. We think there are three dominate mechanisms playing on the DE of TiO_2. One mechanism is that larger E_g would result in reducing photogenerated carriers while less E_g would increase the recombination possibility of photogenerated electron-hole pairs. The second mechanism is the generated internal electrical fields in the nanosized heterogeneous TiO/TiO_2 structures [31]. The internal electrical fields are favors in separating photogenerated electron-hole pairs and prolonging the lifetime of photogenerated carriers [31]. But too much TiO might add the recombination sites of photogenerated electron-hole pairs [35]. The third mechanism is that the more the incorporated TiO is, the larger the Vis absoption is. The combined action of the three mechanisms has resulted in that the DE and PDR of TT20 are the maximum among the as-prepared samples.

Although [36] mentioned that nitrogen- (N-) doped TiO with ~8 nm has efficient photoactivity under UV and visible irradiation, the nanosized TiO with 13 nm in our work shows no considerable photoactivity under UV-Vis irradiation. The considerable response to UV-Vis in [36] probably results from the dopant N. It was reported that the dopant N can add additional energy levels in energy band gap and improve the photocatalytic properties of TiO_2 [37]. Here we think that similar additional levels appear in N-doped TiO and lead to the UV-Vis response.

TiO has much higher EWF than that of TiO_2. Thus, it introduces an easy route for carriers to transfer from the inside to the outside of TiO_2 particles to participate in photocatalytic activity. Consequently, an appropriate content

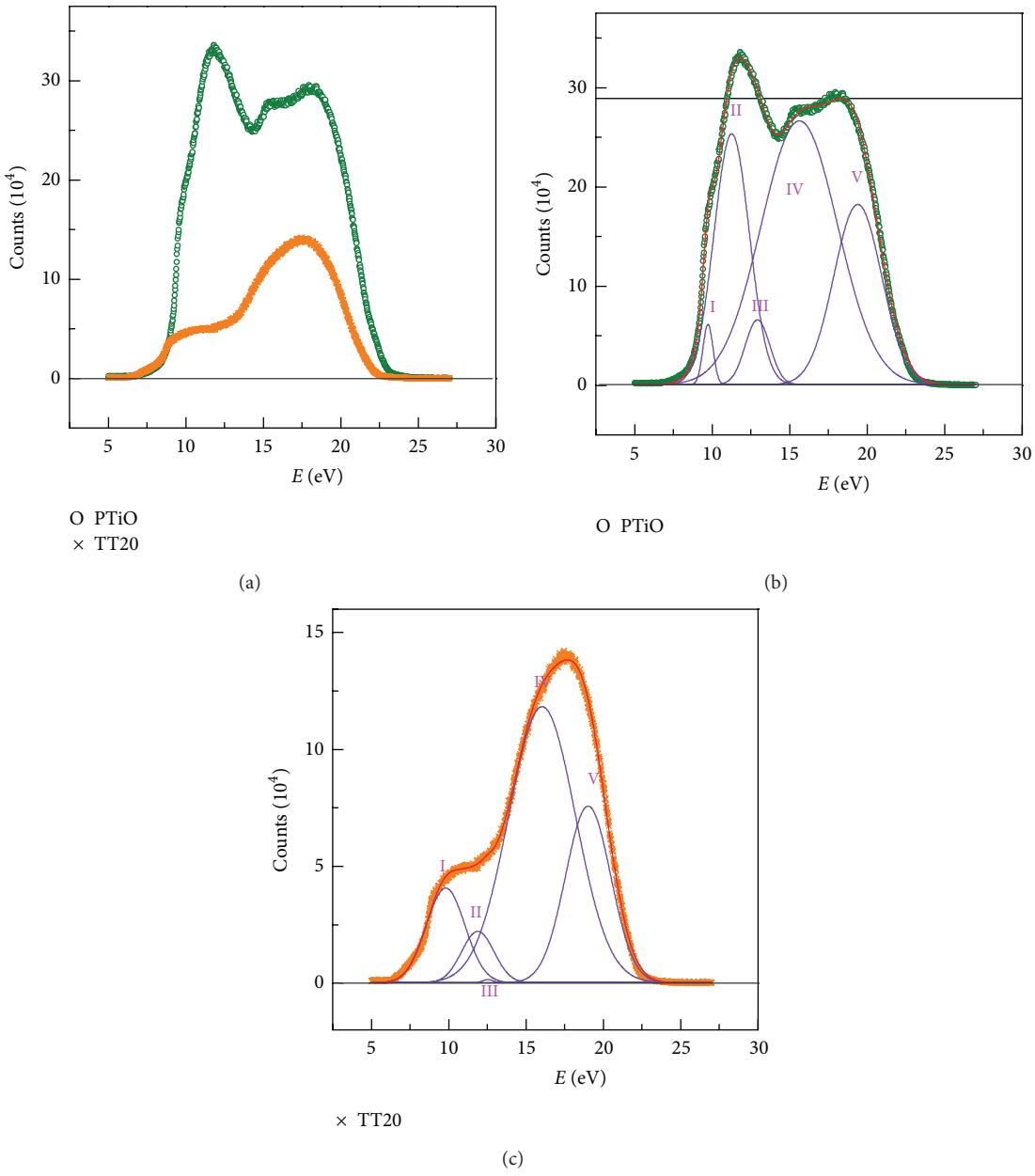

Figure 6: (a) UPS spectra for PTiO and TT20 and (b) and (c) five fitted peaks (labeled by numbers I, II, III, IV, and V) of UPS spectra of PTiO and TiO_2, respectively. The five peaks were fitted based on the expected contributions from the molecular orbitals that comprise the valence bonding states, respectively.

of the incorporated TiO can increase the photocatalytic activity of anatase TiO_2. Furthermore, TiO can enhance the Vis absoption. TiO-incorporated TiO_2 has maximum degradation efficiency of 93%. However this value is less than that in noble metal incorporated TiO_2, for example, 97% in Ag-incorporated TiO_2 system and 100% in Au-incorporated TiO_2 [7, 9, 38]. But the photocatalytic activity of TiO-incorporated TiO_2 is much higher than that of Ag-incorporated TiO_2. In [7, 38], Ag-incorporated TiO_2 took 2 hrs to reach DE of 97% and Au-incorporated TiO_2 took 50 mins to reach DE of 100%. While in this work, TT20 just took 38 mins to reach DE of 93%. Therefore, the TiO-incorporated TiO_2 has much application value.

4. Conclusion

In this work, we employed high-energy ball-milling method to fabricate TiO/TiO_2 heterogeneous nanostructures. XRD proved the existence of TiO/TiO_2 heterogeneous structures. SEM and HRTEM investigation evidenced that the mean particle size and mean grain size of the as-prepared samples

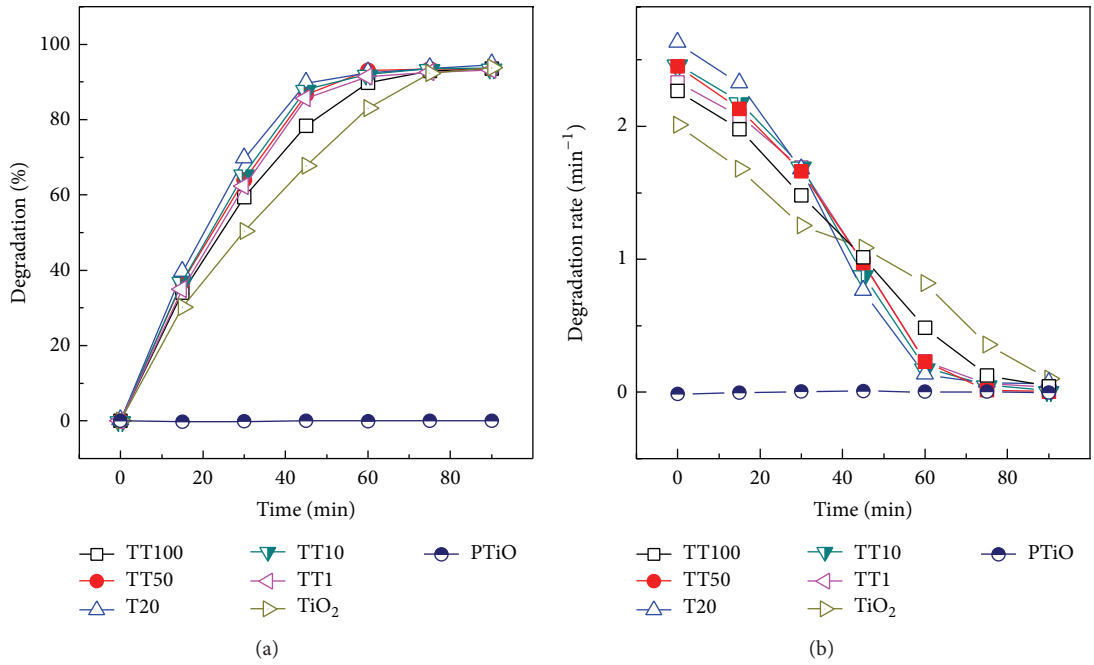

Figure 7: (a) Degradation and (b) degradation rate of the as-prepared samples.

are 23 nm and 13 nm, respectively. UV-Vis exhibited that the incorporated TiO has enhanced the Vis absoption of TiO_2 and has changed the E_g of TiO_2. UPS examination found that the electron work function of TiO is higher than that of TiO_2. Photocatalytic experiment has revealed that an appropriate TiO content can lift the photocatalytic activity of pure TiO_2 to a level better than that of Au-incorporated TiO_2 by keeping high degradation efficiency of 93%. The internal electrical field produced by TiO/TiO_2 heterogeneous nanostructures was thought to be dominantly responsible for the enhanced photocatalytic activity. Therefore, the substitution of the noble metal with TiO to enhance the photocatalytic activity of TiO_2 has much application value. This work also gives a clear direction of enhancing photocatalytic activity of TiO_2 by incorporating a second compound into TiO_2 particle with an appropriate content if the second compound has much higher electron work function than that of TiO_2.

Conflict of Interests

The authors declare that there is no conflict of interests regarding the publication of this paper.

Acknowledgments

This work was financially supported by the National Natural Science Foundation of China (Grant nos. 51172078 and 51372092) and the Guangzhou Science and Technology Project of China (Grant no. 2013J4100045).

References

[1] S. Klosek and D. Raftery, "Visible light driven V-doped TiO_2 photocatalyst and its photooxidation of ethanol," *Journal of Physical Chemistry B*, vol. 105, no. 14, pp. 2815–2819, 2001.

[2] C. F. Guo, J. M. Zhang, M. Wang, Y. Tian, and Q. Liu, "A Strategy to prepare wafer scale bismuth compound superstructures," *Small*, vol. 9, pp. 2394–2398, 2013.

[3] C. F. Guo, J. M. Zhang, Y. Tian, and Q. Liu, "A general strategy to superstructured networks and nested self-similar networks of bismuth compounds," *ACS Nano*, vol. 6, pp. 8746–8752, 2012.

[4] C. F. Guo, S. Cao, J. Zhang et al., "Topotactic transformations of superstructures: from thin films to two-dimensional networks to nested two-dimensional networks," *Journal of the American Chemical Society*, vol. 133, no. 21, pp. 8211–8215, 2011.

[5] S. W. Bae, P. H. Borse, S. J. Hong et al., "Photophysical properties of nanosized metal-doped TiO_2 photocatalyst working under visible light," *Journal of the Korean Physical Society*, vol. 51, no. 1, pp. S22–S26, 2007.

[6] J. Araña, A. Peña Alonso, J. M. Doña Rodríguez, J. A. Herrera Melián, O. González Díaz, and J. Pérez Peña, "Comparative study of MTBE photocatalytic degradation with TiO_2 and Cu-TiO_2," *Applied Catalysis B*, vol. 78, no. 3-4, pp. 355–363, 2008.

[7] X. Z. Li and F. B. Li, "Study of Au/Au^{3+}-TiO_2 photocatalysts toward visible photooxidation for water and wastewater treatment," *Environmental Science & Technology*, vol. 35, no. 11, pp. 2381–2387, 2001.

[8] Ch. Girginov, P. Stefchev, P. Vitanov, and Hr. Dikov, "Silver doped TiO_2 photo-catalyst for methyl orange degradation," *Journal of Engineering Science and Technology Review*, vol. 5, no. 4, pp. 14–17, 2012.

[9] K. Zakrzewska, M. Radecka, A. Kruk, and W. Osuch, "Noble metal/titanium dioxide nanocermets for photoelectrochemical applications," *Solid State Ionics*, vol. 157, no. 1–4, pp. 349–356, 2003.

[10] P. Wei, J. W. Liu, and Z. H. Li, "Effect of Pt loading and calcination temperature on the photo-catalytic hydrogen production activity of TiO_2 microspheres," *Ceramics International*, vol. 39, pp. 5387–5391, 2013.

[11] Z. Zhang and J. T. Yates Jr., "Band bending in semiconductors: chemical and physical consequences at surfaces and interfaces," *Chemical Reviews*, vol. 112, pp. 5520–5551, 2012.

[12] J. M. Schoen and S. P. Denker, "Band structure, physical properties, and stability of TiO by the augmented-plane-wave virtual-crystal approximation," *Physical Review*, vol. 184, no. 3, pp. 864–873, 1969.

[13] S. P. Denker, "Electronic properties of titanium monoxide," *Journal of Applied Physics*, vol. 37, no. 1, pp. 142–149, 1966.

[14] K. I. Saitow and T. J. Wakamiya, "130-fold enhancement of TiO_2 photo-catalytic activities by ball milling," *Applied Physics Letters*, vol. 103, no. 3, pp. 031916–031920, 2013.

[15] S. Al-Qaradawi and S. R. Salman, "Photocatalytic degradation of methyl orange as a model compound," *Journal of Photochemistry and Photobiology A*, vol. 148, no. 1–3, pp. 161–168, 2002.

[16] M. Ge, C. Guo, X. Zhu et al., "Photocatalytic degradation of methyl orange using ZnO/TiO_2 composites," *Frontiers of Environmental Science and Engineering in China*, vol. 3, no. 3, pp. 271–280, 2009.

[17] X. Cheng, X. Yu, and Z. Xing, "One-step synthesis of visible active C N S-tridoped TiO_2 photocatalyst from biomolecule cystine," *Applied Surface Science*, vol. 258, pp. 7644–7650, 2012.

[18] T. Puangpetch, T. Sreethawong, S. Yoshikawa, and S. Chavadej, "Synthesis and photocatalytic activity in methyl orange degradation of mesoporous-assembled $SrTiO_3$ nanocrystals prepared by sol-gel method with the aid of structure-directing surfactant," *Journal of Molecular Catalysis A*, vol. 287, no. 1-2, pp. 70–79, 2008.

[19] N. Barka, S. Qourzal, A. Assabbane, and Y. Ait-Ichou, "Kinetic modeling of the photo-catalytic degradation of methyl orange by supported TiO_2," *Journal of Environmental Science and Engineering*, vol. 4, no. 5, pp. 1–4, 2010.

[20] A. E. Belyaev, N. V. Shevchenko, and Z. A. Demidenko, "Free carrier absorption in narrow-gap semiconductors," *Journal of Infrared and Millimeter Waves*, vol. 10, no. 4, pp. 241–245, 1991.

[21] N. Serpone, D. Lawless, and R. Khairutdinov, "Size effects on the photophysical properties of colloidal anatase TiO_2 particles: size quantization or direct transitions in this indirect semiconductor?" *Journal of Physical Chemistry*, vol. 99, no. 45, pp. 16646–16654, 1995.

[22] E. Mooser and W. B. Pearson, *Progress in Semiconductors*, vol. 5, John Wiley & Sons, New York, NY, USA, 1960, Edited by A.F. Gibson.

[23] K. M. Reddy, S. V. Manorama, and A. R. Reddy, "Bandgap studies on anatase titanium dioxide nanoparticles," *Materials Chemistry and Physics*, vol. 78, no. 1, pp. 239–245, 2003.

[24] A. R. Kumarasinghe, W. R. Flavell, A. G. Thomas et al., "Electronic properties of the interface between p-CuI and anatase-phase n-TiO_2 single crystal and nanoparticulate surfaces: a photoemission study," *Journal of Chemical Physics*, vol. 127, no. 11, Article ID 114703, pp. 114703–114717, 2007.

[25] M. Fernández-García, X. Wang, C. Belver, J. C. Hanson, and J. A. Rodriguez, "Anatase-TiO_2 nanomaterials: morphological/size dependence of the crystallization and phase behavior phenomena," *Journal of Physical Chemistry C*, vol. 111, no. 2, pp. 674–682, 2007.

[26] V. Senthilkumar, M. Jayachandran, and C. Sanjeeviraja, "Preparation of anatase TiO_2 thin films for dye-sensitized solar cells by DC reactive magnetron sputtering technique," *Thin Solid Films*, vol. 519, no. 3, pp. 991–994, 2010.

[27] Y. V. Kolen'ko, A. V. Garshev, B. R. Churagulov, S. Boujday, P. Portes, and C. Colbeau-Justin, "Photocatalytic activity of sol-gel derived titania converted into nanocrystalline powders by supercritical drying," *Journal of Photochemistry and Photobiology A*, vol. 172, no. 1, pp. 19–26, 2005.

[28] R. J. Tayade, H. C. Bajaj, and R. V. Jasra, "Photocatalytic removal of organic contaminants from water exploiting tuned bandgap photocatalysts," *Desalination*, vol. 275, no. 1–3, pp. 160–165, 2011.

[29] L. Vayssieres, C. Persson, and J.-H. Guo, "Size effect on the conduction band orbital character of anatase TiO_2 nanocrystals," *Applied Physics Letters*, vol. 99, no. 18, Article ID 183101, 2011.

[30] S. Monticone, R. Tufeu, A. V. Kanaev, E. Scolan, and C. Sanchez, "Quantum size effect in TiO_2 nanoparticles: does it exist?" *Applied Surface Science*, vol. 162-163, pp. 565–570, 2000.

[31] F. A. Cotton, *Chemical Applications of Group Theory*, Wiley-Interscience, New York, NY, USA, 3rd edition, 1990.

[32] T. Ioannides and V. P. Zhdanov, "Comment on: 'Nm-sized metal particles on a semiconductor surface, Schottky model, and i.e.' by V.P. Zhdanov [Surf. Sci. 512 (2002) L331–L334]," *Surface Science*, vol. 530, no. 3, pp. 216–220, 2003.

[33] N. Barka, S. Qourzal, A. Assabbane, and Y. Ait-Ichou, "Kinetic modeling of the photocatalytic degradation of methyl orange by supported TiO_2," *Journal of Environmental Science and Engineering*, vol. 5, no. 30, pp. 1–5, 2010.

[34] M. N. Rashed and A. A. EI-Amin, "Photocatalytic degradation of methyl orange in aqueous TiO_2 under different solar irradiation sources," *International Journal of Physical Sciences*, vol. 2, pp. 73–81, 2007.

[35] J. F. Lei, X. P. Li, W. S. Li, F. Q. Sun, D. S. Lu, and Y. Lin, "Photocatalytic degradation of methyl orange on arrayed porous iron-doped anatase TiO_2," *Journal of Solid State Electrochemistry*, vol. 16, no. 2, pp. 625–632, 2012.

[36] P. Simon, B. Pignon, B. J. Miao et al., "N-doped titanium monoxide nanoparticles with TiO rock-salt structure, low energy band gap, and visible light activity," *Chemistry of Materials*, vol. 22, no. 12, pp. 3704–3711, 2010.

[37] M. Batzill, E. H. Morales, and U. Diebold, "Influence of nitrogen doping on the defect formation and surface properties of TiO_2 rutile and anatase," *Physical Review Letters*, vol. 96, no. 2, pp. 026103–026106, 2006.

[38] R. Nainani, P. Thakur, and M. Chaskar, "Synthesis of silver doped TiO_2 nanoparticles for the improved photocatalytic degradation of methyl orange," *Journal of Materials Science and Engineering B*, vol. 2, pp. 52–58, 2012.